Origami Solar-Tracking Concentrators

Tainon Chen

Professor Pei-Cheng Ku

Summary

The field of solar cells has conventionally been dominated by crystalline silicon, owing to its low cost. Alternative semiconductor materials are typically prohibitively priced, but recent developments are slowly improving their feasibility.

This project explores one such option, by incorporating compound parabolic reflective concentrators into solar cell design. Different 2D designs were constructed, and their light collection simulated, using Matlab. The concentrators were optimized for power output. Future research will convert high-performing 2D designs to 3D ones, to better understand the real-world performance of the concentrators.

Introduction

Solar Cells

Solar panels are one of the fastest-growing sources of renewable energy, having experienced accelerated growth the past few years. As demand for solar panels increase, so too does the importance of improving efficiency of solar panels.

Solar cells convert sunlight into electricity due to the photovoltaic nature of the semiconductors they contain. Absorbing an incoming photon results in an electron-hole pair being generated in the semiconductor. The ensuing movement of these charge carriers back to their original states generates an electric current.

Feasibility of GaAs Solar Cells

Conventional solar cells utilize crystalline silicon, a relatively inexpensive semiconductor. However, the performance of silicon solar cells is limited by the power efficiency of silicon, defined as the ratio of incoming (solar) power to output power. There exist alternative semiconductor materials with greater efficiencies, but they which are typically prohibitively priced, sometimes reaching costs hundreds or thousands of times greater than silicon. One such example is gallium arsenide (GaAs), which has a raw square-meter cost of approximately $8000, in sharp contrast to the square-meter cost for silicon of around $5.7.

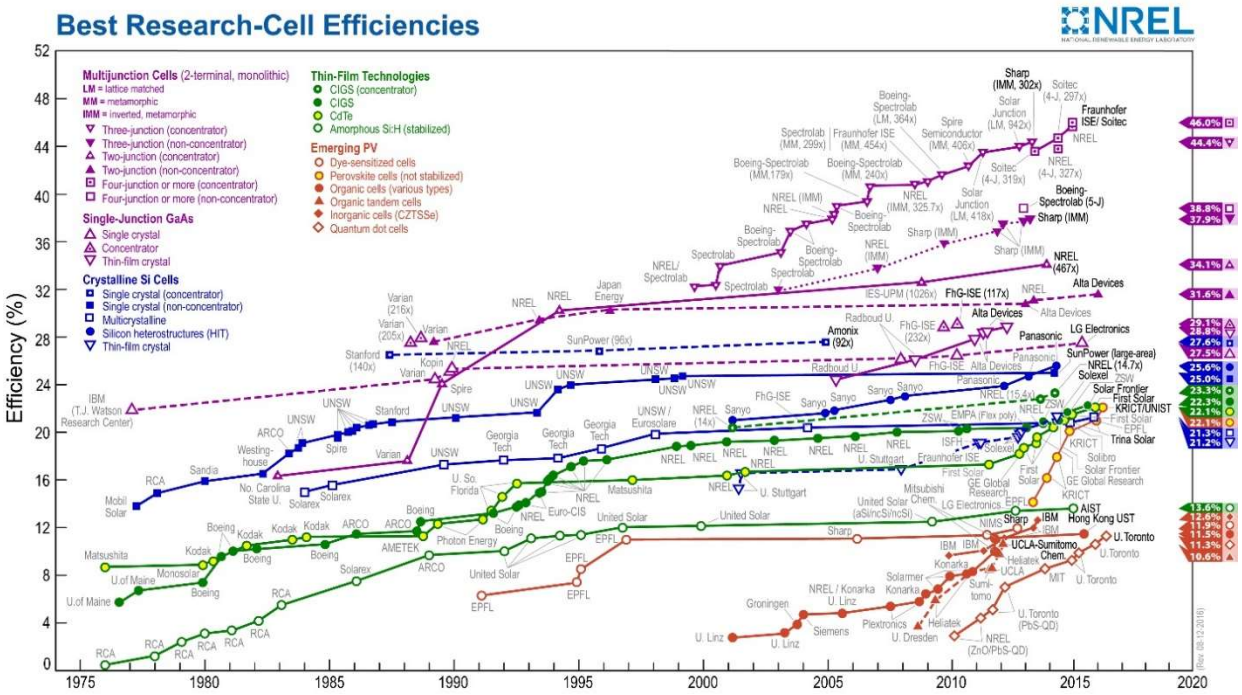

Figure 1: Plot of various solar cell efficiencies over time. The plot includes both Silicon and GaAs solar cells (refer to legend at top-right). It also includes multijunction cells, which are referenced later in this section. Note the general upward trend for the efficiencies as time progresses.

However, recent developments in semiconductor and solar cell efficiency has made the use of more expensive semiconductors, such as GaAs, a possibility. These developments occur on both the semiconductor side and light collection side. Utilizing them together drastically reduces the cost of GaAs solar cells, to the point that their cost is below that of benchmarks typically used for conventional solar panels.

On the semiconductor side, a process called non-destructive epitaxial lift-off (ND-ELO) was recently developed, which reduces the cost of creating GaAs solar cells. This process prevents degradation of the semiconductor substrate used to create the thin semiconductor sheets utilized in solar cells. This allows for much greater reuse of the host substrate. When combined with other technologies, such as multi-junction solar cells, which include layers of different semiconductors within the same solar cell to improve efficiency, it becomes significantly cheaper to develop these more efficient GaAs solar cells.

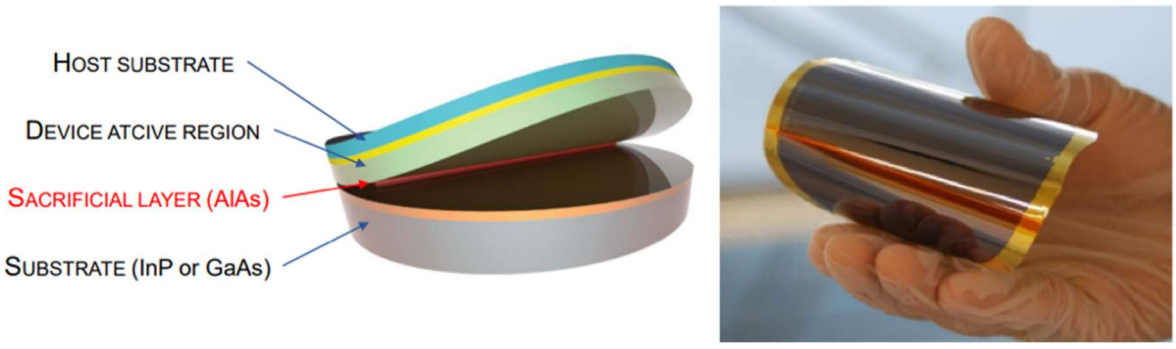

Figure 2: A cross-section of a ND-ELO solar cell shown on the left, and an actual solar cell produced using ND-ELO shown on the right.

There have also been improvements present in optimizing light collection of solar cells. One such method is the use of solar concentrators, with a tracking array. Concentrators, made of reflective material, redirect incoming sunlight to the semiconductor located at their base. This allows for less total semiconductor material to be used, while retaining light collection over a large area. However, unlike conventional flat solar panels, concentrators are more sensitive to changes in incoming sunlight angle. As such, they are typically implemented with a tracking array, which ensures that the concentrator stays pointed in the correct angle relative to incoming sunlight.

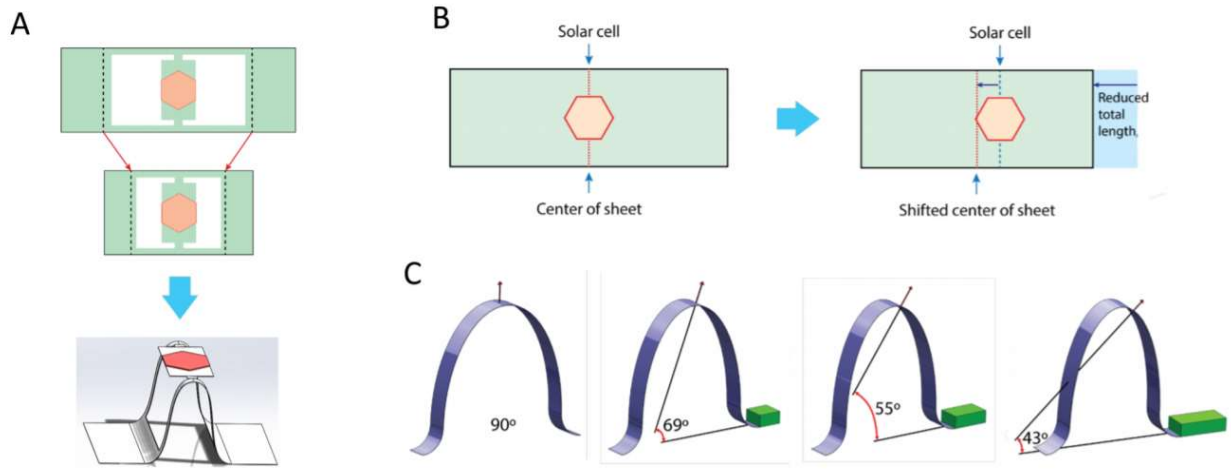

Figure 3: Renditions of a single tracker on the tracking array. The hexagon is the semiconductor base of the concentrator. It is fixed to the tracker. The angle of the tracker can be adjusted using an attached actuator (shown as a green box), which changes the curvature of the tracker, and in turn tilts the semiconductor at the corresponding angle. The current tracking array design can tilt the concentrator 60 degrees in either direction.

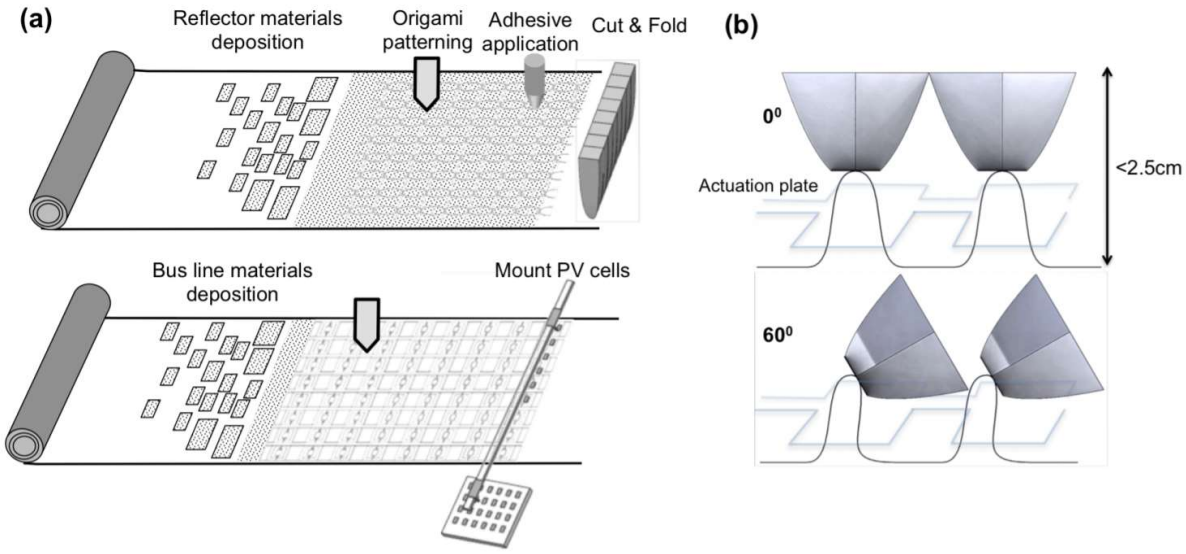

Figure 4: A full tracking array, consisting of multiple trackers arranged in a grid, is seen on the left. A pair of trackers, with concentrator affixed, is seen on the right. Note that the semiconductor base in *Figure 3* is located at the bottom of the concentrators.

Concentrator Design

The primary focus of this project was centered around optimizing the concentrator design. We sought to create a concentrator which maximized the light collected, while minimizing the amount of semiconductor material required. Additionally, we strove to make the design easy to manufacture, using a cut-and-fold method which should minimize the cost of production.

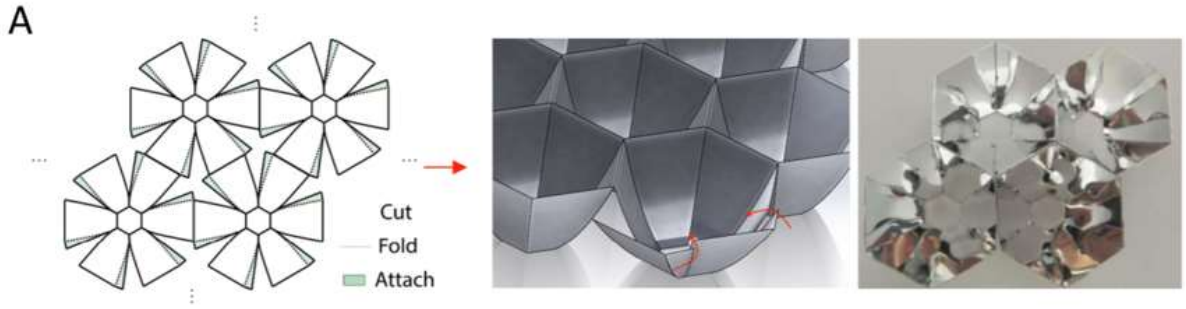

Figure 5: Depiction of a hexagonal concentrator. This design allows for an array of concentrators to be created from a single sheet of reflective material, by cutting and folding the material at specific points.

There were two primary concentrator designs which were of interest to this project. The first was a simple parabolic design. Simple parabolic concentrators exploit the optical nature of the parabola to collect light. Parabolas redirect all rays perpendicular to their axis to their focal point. However, even minor deviations in incoming light angle will result in this no longer being true. As such, parabolic concentrators may seem ideal on the theoretical side, but are not very

practical. The only parameter which can be tweaked for simple parabolic concentrators is the shape of the parabola, determined by the parabola coefficient. This would change the curvature of the parabola, and the location of the focus.

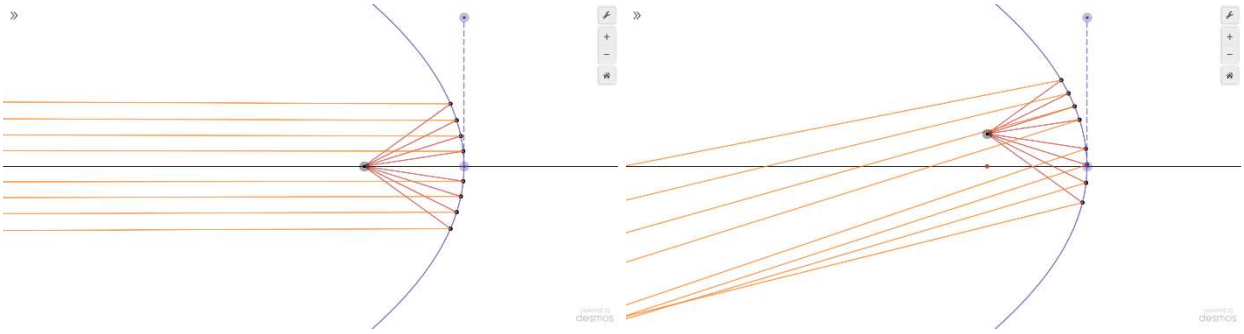

Figure 6: Light collection of a parabola. Optimal case is shown on the left, and suboptimal case is shown on the right. In the second case, the incoming rays are now directed to another point, no longer the focus.

The second concentrator design, and the primary focus of the project, was a compound parabolic design. Compound parabolic concentrators also take advantage of the light-focusing properties of the parabolic shape. Two overlapping parabolas are rotated in opposite directions, and their overlap used to create a concentrator. This grants a higher degree of flexibility in concentrator design, since it introduces new parameters which can be adjusted. Additionally, this allows for the concentrator to collect light entering at different angles, rather than just light entering perpendicular to the base. This makes the design more robust – The concentrator no longer has to be pointed exactly at the sun using the tracking array, and slight deviations will not severely impact performance.

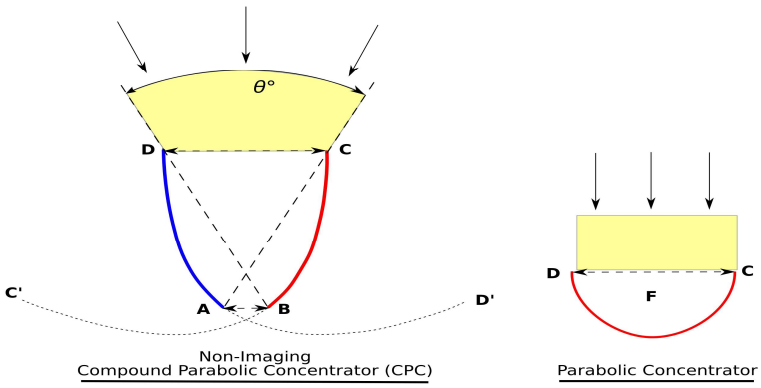

Figure 7: Light collection of different parabolic concentrators. The compound parabolic concentrator, shown on the left, can collect light from a greater variety of angles than the simple parabolic concentrator, shown on the right.

The aforementioned simple and compound parabolic designs both have to be translated to three-dimensional concentrators to use in the real world. For simple parabolic concentrators, this typically involves a conic-section rotation around the center axis, yielding an object similar to a rounded cone. The base is placed at the same depth as the focus.

An ideal compound parabolic design would follow the same circular rotation to yield a real-world concentrator. However, such a circular design would be difficult to manufacture cheaply. Instead, we investigate using polygonal designs, rather than circular ones. These designs would enable a cut-and-fold manufacturing process, but are not as effective as the circular designs, due to light collection being less effective at the edges. A previous project employed hexagonal bases – This project proposes square designs as an alternative.

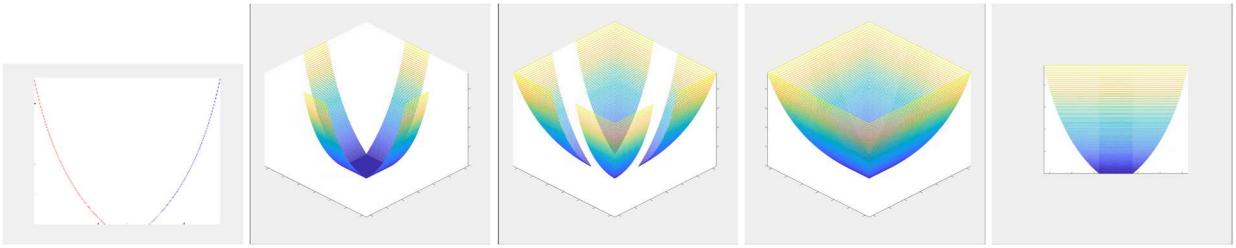

Figure 8: Obtaining the square-based three-dimensional compound parabolic concentrator from a corresponding two-dimensional design. The two-dimensional design (first image) is first stretched along a depth axis, then duplicated and rotated 90 degrees (second image). The spaces between these parabolic sections are filled (third image), to obtain a complete concentrator (fourth image). The side view of the three-dimensional concentrator (fifth image) closely resembles the original two-dimensional concentrator.

This project primarily investigated two-dimensional compound parabolic concentrators to determine the optimal design which would maximize light collection, while minimizing the size of the base, which corresponds to how much semiconductor is needed.

Methods

Concentrator Creation

Five parameters were investigated, and their roles on light collection and cost reduction of the concentrators was assessed. Each parameter was involved in the process of creating a 2D concentrator from a pair of parabolas. The parameters were parabola coefficient, rotation angle, separation, base position, and maximum height factor. The figure below illustrates the creation of the concentrator at each step of the process. Matlab was used for all code and plots.

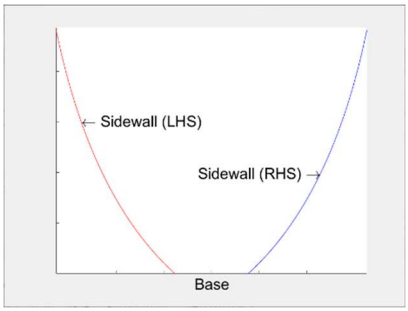

Figure 9: Labeled image of example 2D concentrator. The sides of the concentrator are called the sidewalls, and are made from reflective material. Incoming light is reflected by the sidewalls into the base, made from semiconductor material.

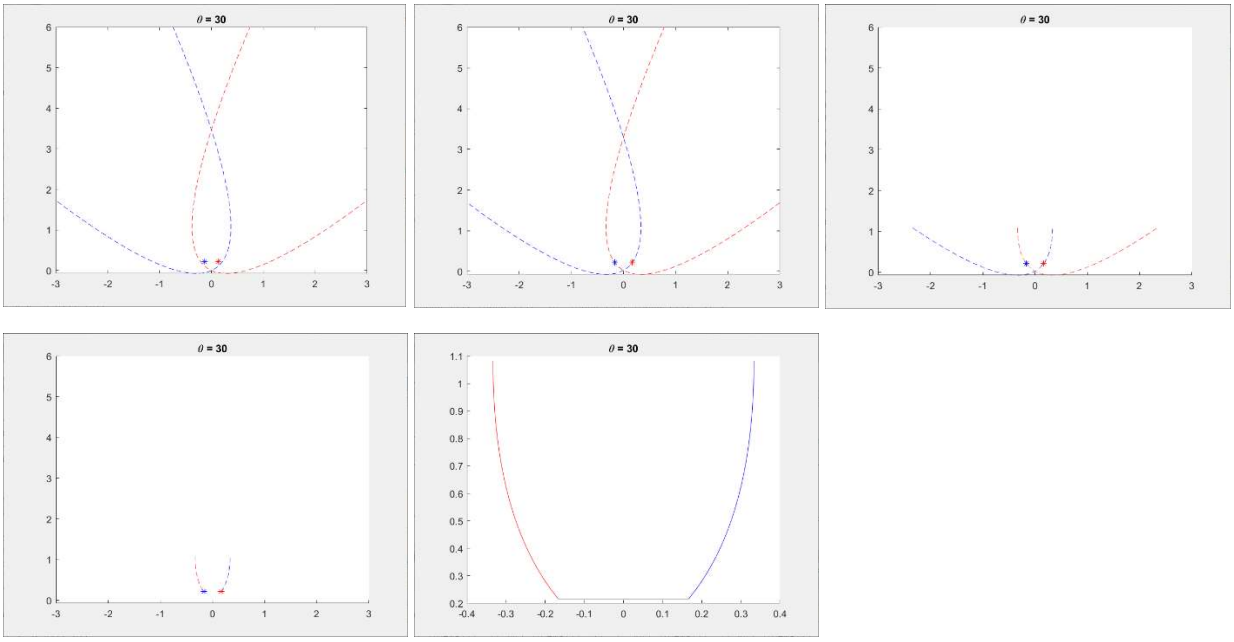

Figure 10: We start off with two overlapping parabolas: red and blue, with their respective foci indicated as asterisks. The parabolas are first rotated in opposite directions by the rotation angle (first image). The possible range of rotation angles is from 0 to 45 degrees. The parabolas are then translated horizontally by the separation value, either towards or away from each other (second image). A positive separation value indicated that the parabolas were moved towards each other, and a negative separation value indicated that the parabolas moved away from each other. Next, the regions of the parabolas where the sidewalls "close in" are removed – an unobstructed aperture is required to maximize light collection (third image). The base is then placed according to the base position (fourth image). This value has a range from 0 to 1. A base position of 0 corresponds to placing the base at the intersection point of the parabolas, essentially resulting in a nonexistent base. A base position of 1 corresponds to placing the base at the very top of the concentrator, resulting in nonexistent sidewalls. Values between 0 and 1 indicate the base placement, proportional from the bottommost position. The final concentrator is shown in the fifth image.

After creating the concentrator in this way, the maximum height factor had to be determined. At the maximum possible height factor of 1, the concentrator is left untouched after placing the base. This would maximize the amount of light collected – by shortening the sidewalls of the concentrator, light which would have entered the concentrator at those regions is no longer collected. However, due to the nature of the tracking array, concentrators are placed in close proximity with each other. This could result in adjacent concentrators colliding while being tilted, if the concentrators are too tall.

Binary search was used to efficiently and accurately determine the maximum possible height for which adjacent concentrators would not collide within the range of rotation of the tracking array. Height factor was thus defined as the ratio of the concentrator height to the unrestricted maximum height. Concentrators were represented as matrices of points, which were then rotated. Collision was assessed by searching for points of intersection between the points meant to represent different concentrators. A brief overview is shown below.

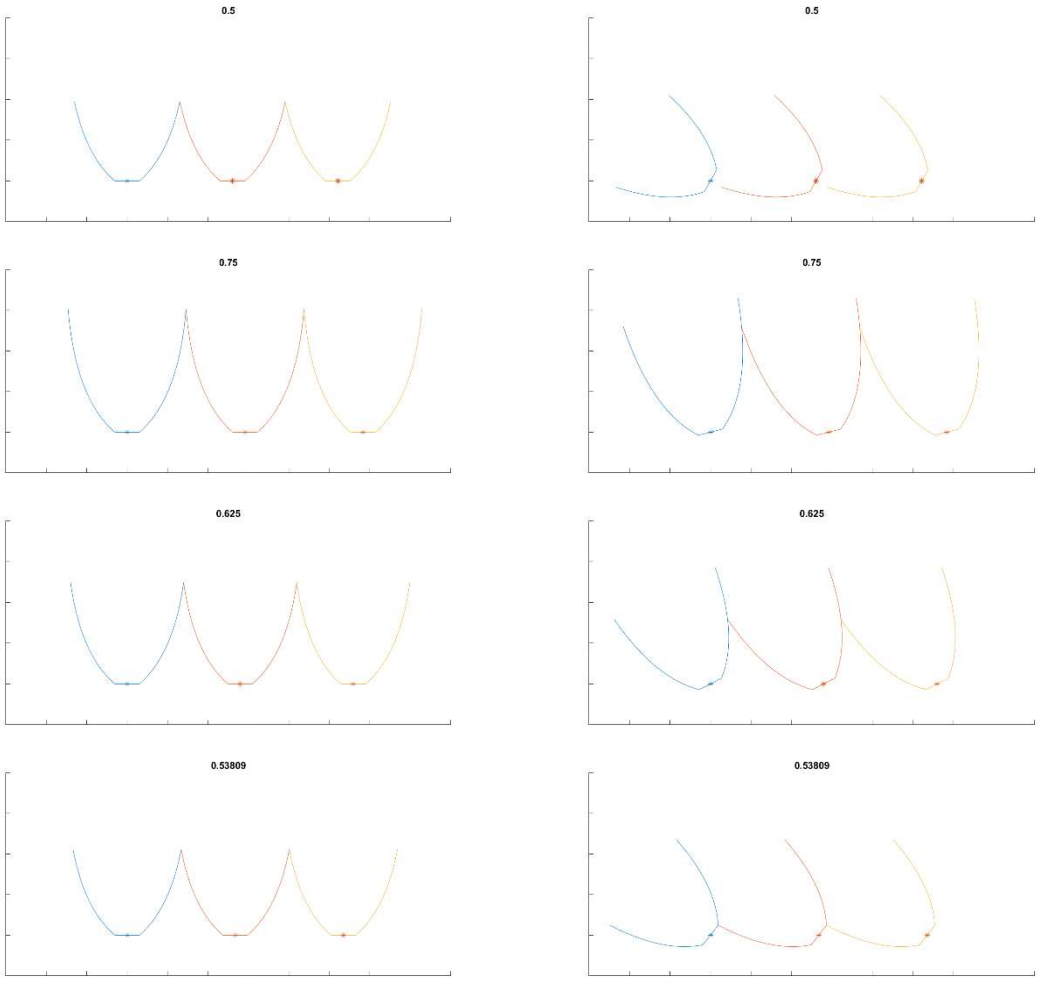

Figure 11: We start off with a height factor of 0.5 (first image). This allows for the concentrators to complete a 60-degree rotation without collision (second image), so we increase the height

factor to 0.75 (third image). However, this now results in a collision (fourth image). We reduce the height factor to 0.625 (fifth image), which still results in a collision (sixth image). After several more iterations, we determine the optimal height factor to be 0.53809 for this particular concentrator (seventh and eighth images).

Simulating Light Collection

After creating the concentrator and determining its optimal height, we next simulate light collection. The guiding principle behind this was the law of reflection – When light collides with a reflective surface, the angle of incidence will equal the angle of reflection. It was assumed that the concentrator sidewalls were perfect reflectors, and thus would redirect light in this manner. For the simulation, rays were generated perpendicular to the base, at set increments at the top of the concentrator. Whenever the rays collided with the sidewall, the new direction was calculated using the law of reflection. If the ray intersects the base, it is collected. If it exits the bounds of the concentrator, it is not collected. This light collection was simulated for concentrators with varied parameters, to obtain each concentrator's light collection ratio: The ratio of rays collected by the base to total rays.

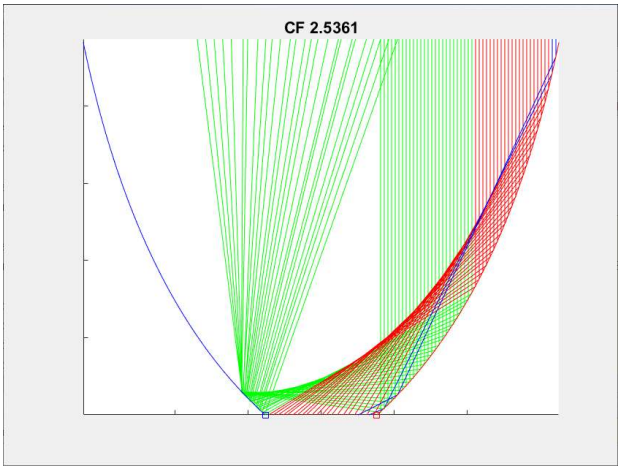

Figure 12: This shows the three different observed behaviors of incoming light. Green rays are not collected – they are reflected to the opposite sidewall, and redirected out of the concentrator. Red rays are collected after intersecting the sidewall exactly once. Blue rays are collected after intersecting the sidewall multiple times.

The primary measure for assessing performance of the concentrators was concentration factor, or CF. It is obtained by multiplying the light collection ratio by the length (area for 3D concentrators) of the top of the concentrator, then dividing this by length (area) of the base of the concentrator. The concentration factor increases as additional light is collected, and decreases as the size of the base increases. The division by the size of the base is meant to penalize concentrators with large bases, which would require larger amounts of semiconductor, and thus be more expensive.

$$CF = \frac{Rays\ Collected}{Total\ Rays} * \frac{Top\ Area}{Base\ Area}$$

The concentration factor of a conventional solar panel, which does not employ a concentrator, is 1. All the rays are collected, and the area of the top is equivalent to the area of the base.

A concentrator able to collect all incoming light, but with a base area that is half the top area, would have a light collection ratio of 1, and a top/base ratio of 2. This results in a concentration factor of 2. This essentially means that for a given amount of semiconductor, this concentrator would be able to generate twice as much power as the solar panel with concentration factor of 1.

If, however, only 80% of incoming light was collected, but retaining the same top area/base area ratio of 2, the concentration factor would now be 1.6, which is still an improvement over the flat solar panel.

The concentration factor was calculated for all concentrators, after determining the light collection ratio using the method detailed earlier.

Results

The effects of each parameter on light collection ratio and top/base ratio, as well as the concentration factor, were analyzed.

It was found that changing the parabola coefficient, while keeping all other parameters constant, had no effect on any of the ratios or CF. This is likely because all parabolas are geometrically similar, meaning that they are interchangeable after shifting and scaling. As such, the concentrators obtained from these parabolas were geometrically similar as well, meaning that both the light collection ratio and top/base ratio are unaffected.

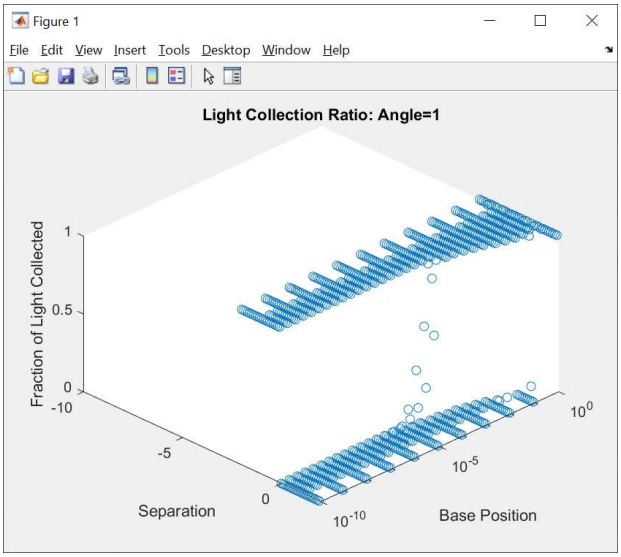

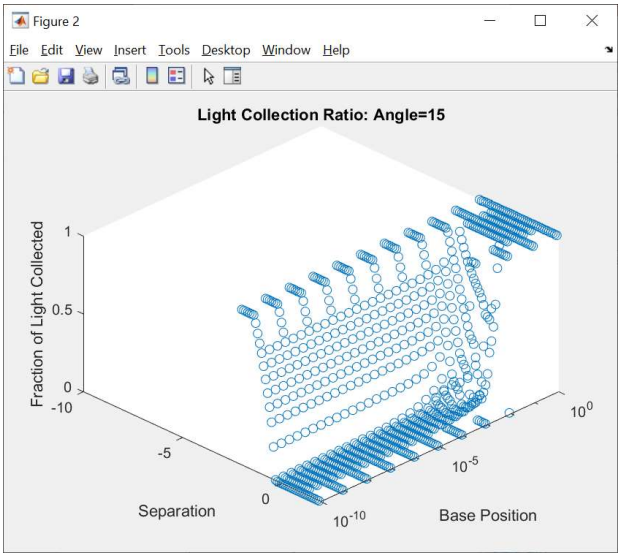

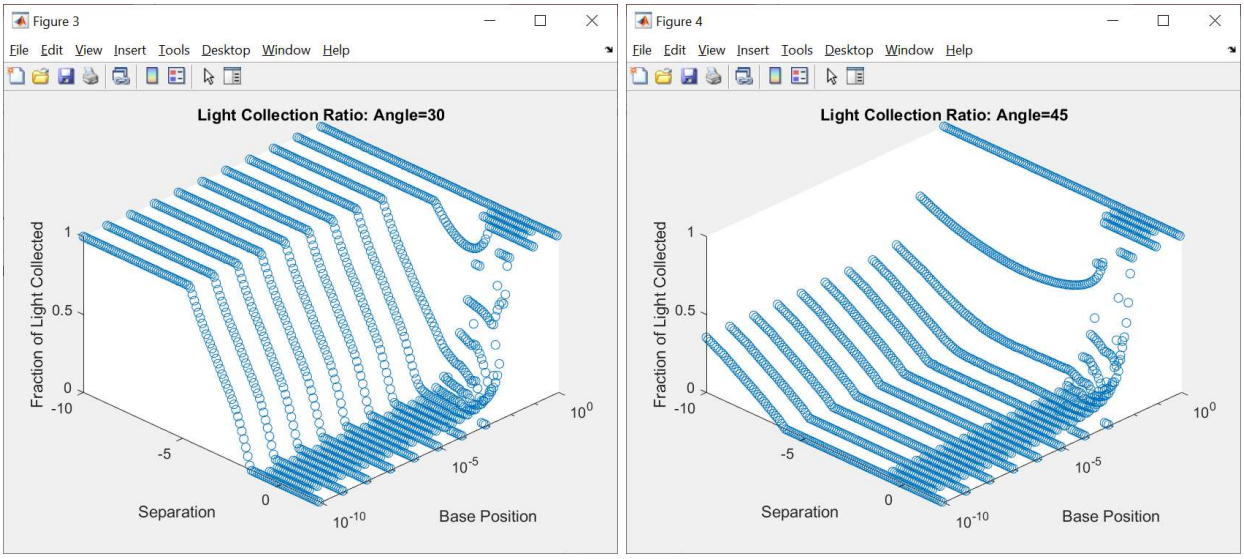

Figure 13: The above graphs show the light collection ratios of concentrators with varied parameters. Each individual graph represents a different angle, and contains concentrators of different base positions and separation factors.

Relative to separation, we observe that light collection starts off at 0, before increasing linearly to 1, for each concentrator. Light collection is likely 0 when the foci of the parabolas are not included in the concentrator. Increasing separation at this point would increase spacing between the concentrators, so that the foci are contained within the concentrator again, at which point light collection is no longer 0. Increasing separation further would increase the length of the base, and therefore potential area that light can be collected, until all incoming light can be collected, resulting in a ratio of 1.

Relative to base position, we observe that the majority of concentrators with the same range of separations, tested at constant base position, are similar. However, near a base position of 1, the light collection ratio approaches a constant 1. This is explained by the fact that a concentrator with base position of 1 has the base placed at the exact top of the concentrator, resulting in a design akin to a solar panel. This would result in all incoming light being collected.

Lastly, as angle increases, the graphs are shown to stretch further along the separation axis. The graph with angle of 1 had the most sudden change in light collection ratio. For the other graphs, with higher angle, the light collection ratio curve just appears to be more and more stretched out.

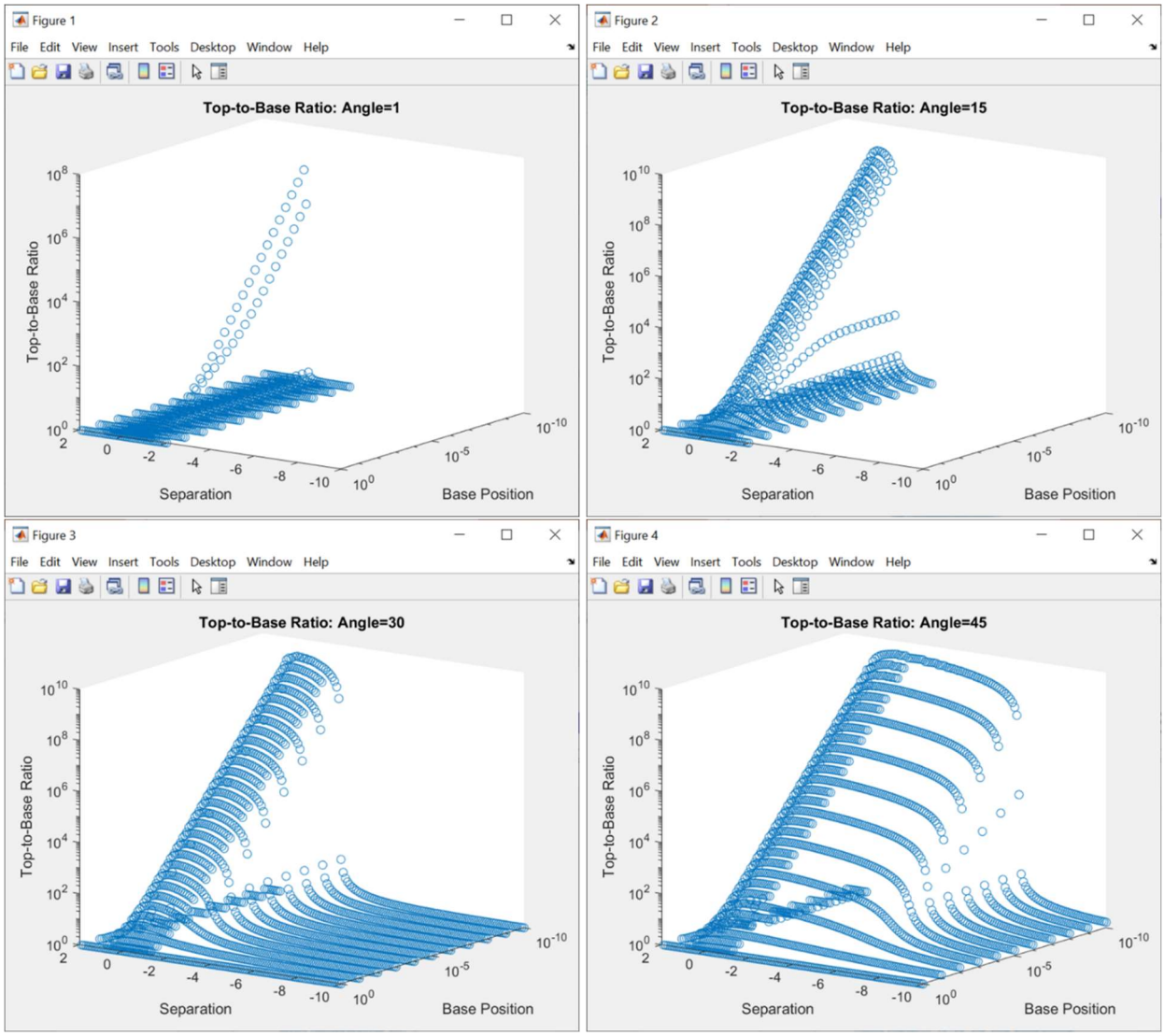

Figure 14: The above graphs show the top/base ratios of concentrators with varied parameters. Each individual graph represents a different angle, and contains concentrators of different base positions and separation factors.

Relative to separation, we observe that top/base ratio starts off low, increases, then decreases back down to 1. At high separations, the concentrator will more closely resemble a flat solar panel. Peak top/base ratio for each curve was likely more dependent on base position than separation, although they typically occurred at similar separation values.

Relative to base position, the top/base ratio increases in the same ratio as the base position decreases. This makes sense, as decreasing the base position by a certain factor would decrease base size by that same factor, which would in turn increase top/base ratio by that factor. When the base position was 1, the top/base ratio was a consistent 1, which is what we expected to observe.

Lastly, similar to the light collection plots, as angle increases, the graphs are shown to stretch further along the separation axis. The graph with angle of 1 had the most sudden change in top/base ratio. For the other graphs, with higher angle, the curves just appears to be more and more stretched out.

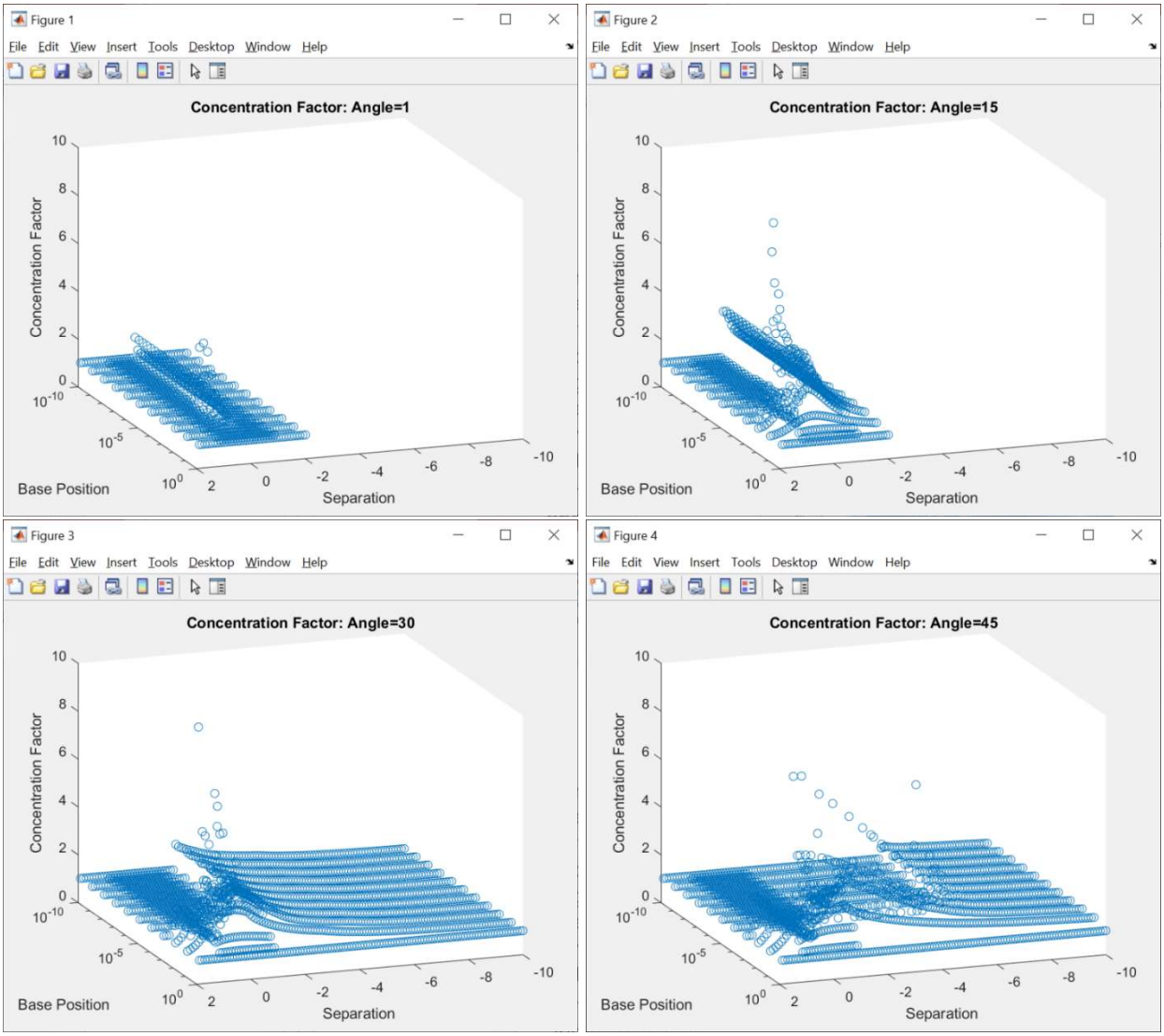

Figure 15: The above graphs show the concentration factors of concentrators with varied parameters. Each individual graph represents a different angle, and contains concentrators of different base positions and separation factors.

Relative to separation, we observe that concentration factor increases from 1 in a gradual curve, then drops back down to 1. Concentration factors for base position of 1 was also a constant 1. It experiences a few higher peaks near these base positions, then as it decreases, the concentration factor becomes constant. Lastly, as concentration factor is the product of light collection ratio and top/base ratio, it is not surprising that similar to the other two, as angle increases, the graphs are shown to stretch further along the separation axis. The graph

with angle of 1 had the most sudden change in concentration factor. For the other graphs, with higher angle, the curves just appears to be more and more stretched out.

Conclusion

This project explored how changing different parameters of 2D compound parabolic concentrators would affect their light collection ability, as measured in concentration factor. A number of trends were identified, as well as the regions where the concentration factor appears to be the highest.

The next steps of this project will involve converting the concentrators with highest concentration factor to the square-based three dimensional design, and analyze their light collection ability to ensure that it resembles their 2D concentration factor. Additionally, the concentration factor calculated from Matlab can be verified by using Multiphysics software, such as COMSOL, to simulate light collection.

Appendices

This includes brief explanations for key highlights in the final code used in obtaining results, as well as why they were developed.

Appendix A: Explicit Concentrator Equations

Using the rotation matrix and equation of a parabola, we can solve for an explicit equation for the rotated parabola, in the form y=f(x). The advantage of doing so is to retain constant distance between the points of the concentrator, regardless of the rotation angle. The original method of rotating the points of a parabola directly would result in consistent spacing only when unrotated – after rotating, spacing no longer is consistent, which can lead to parts of the concentrator being more densely populated with points than others.

Wolfram Mathematica was used to solve for equations in terms of y. They are listed below:

```
RHS:
y1=(1/2)*B^(-1)*((-2)*B*d*cot(p)+2*B*x*cot(p)+cot(p)*csc(p)+(-1)
*2^(-1/2)*csc(p)^2*(1+cos(2*p)+(-8)*B*d*sin(p)+8*B*x*sin(p))
^(1/2));
y2=(1/2)*B^(-1)*((-2)*B*d*cot(p)+2*B*x*cot(p)+cot(p)*csc(p)
+2^(-1/2)*csc(p)^2*(1+cos(2*p)+(-8)*B*d*sin(p)+8*B*x*sin(p))
^(1/2));
LHS:
y1=(1/2)*B^(-1)*((-2)*B*x*cot(p)+cot(p)*csc(p)+(-1)*2^(-1/2)
*csc(p)^2*(1+cos(2*p)+(-8)*B*x*sin(p))^(1/2));
y2=(1/2)*B^(-1)*((-2)*B*x*cot(p)+cot(p)*csc(p)+2^(-1/2)
*csc(p)^2*(1+cos(2*p)+(-8)*B*x*sin(p))^(1/2));
```

Note that there are two equations for both the RHS (right-hand sidewall) and LHS (left-hand sidewall). This is because after rotating, the parabolas are no longer considered functions, since multiple y-coordinates can share the same x-coordinate. However, after plotting, it becomes clear that these are in fact the equations of the concentrator.

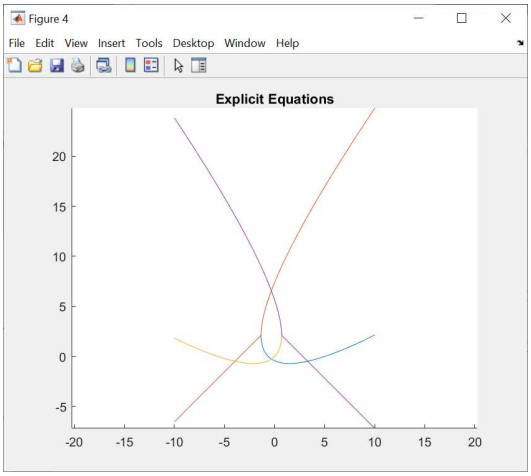

In the above figure, the blue line corresponds to RHS y1, red is RHS y2, yellow is LHS y1, and purple is LHS y2. For the concentrator, the equations of interest are RHS y1 and LHS y1, the blue and yellow plots. The y2 plots are not present until the sidewalls have started to "close in", and contain the section of the concentrator which would be trimmed off through normal means.

Appendix B: Calculating Concentrator Intersection

The Matlab function InterX was used to determine whether or not adjacent concentrators collided while performing binary search to find the optimal height factor. It can be found at the following link: https://www.mathworks.com/matlabcentral/fileexchange/22441-curve-intersections

InterX runs relatively fast, and is able to interpolate intersection points, as shown below.

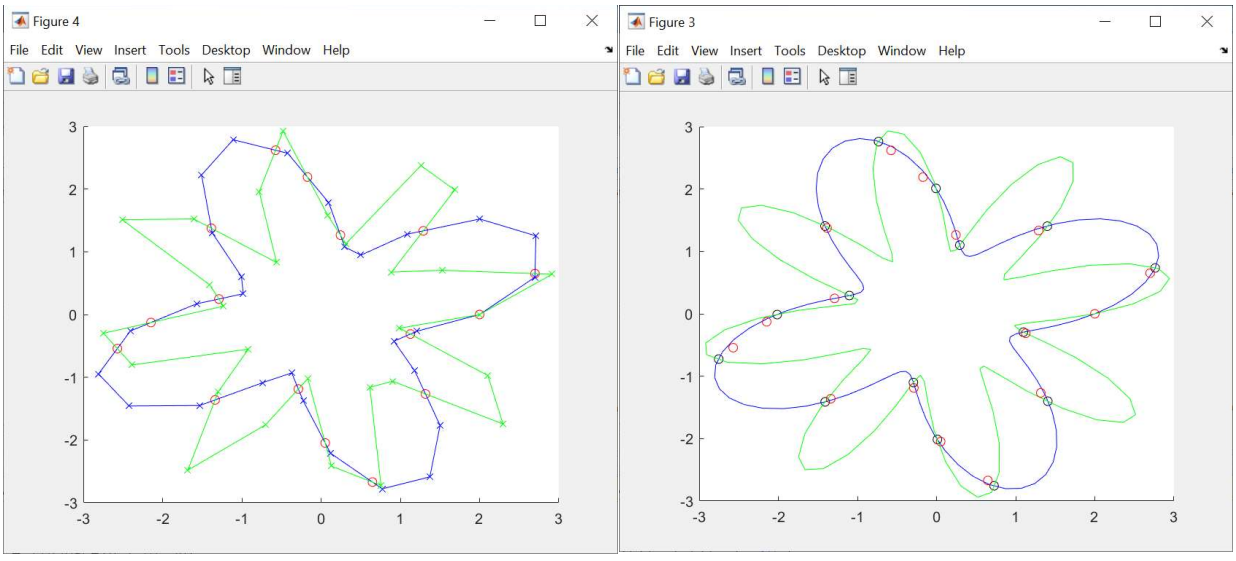

On the left is a relatively sparse plot – only points which were graphed are indicated as x's. InterX assumes that all connecting segments are linear, and returns the points where each intersection occurs as a red circle.

The plot on the right features the same equation, but with much higher resolution. The red intersection points are carried over from the plot on the left. We can see that the actual intersection points, indicated in blue, are mismatched from the points in red. This is due to InterX being limited by the resolution of the data from the left plot.

Therefore, it should be kept in mind that InterX is only as accurate as the data points provided to it, and that large gaps between data points should be avoided. Implementing the code using explicit concentrator equations (Appendix A) was helpful in this regard.

Appendix C: Optimizing Concentrator Intersection Detection

Running InterX for concentrators with many points can result in a long runtime. After observing that collisions between concentrators occurred only at the top of the concentrator, or where the sidewall meets the base, the code was modified to only use a higher resolution of points at these two regions.

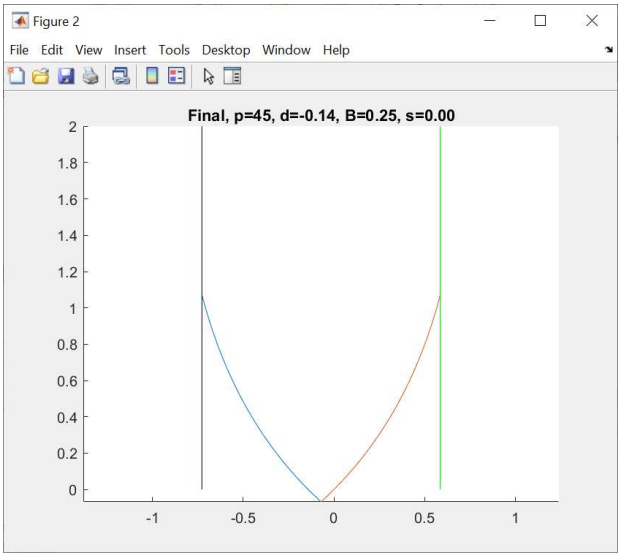

This is an example concentrator, with a very low base position.

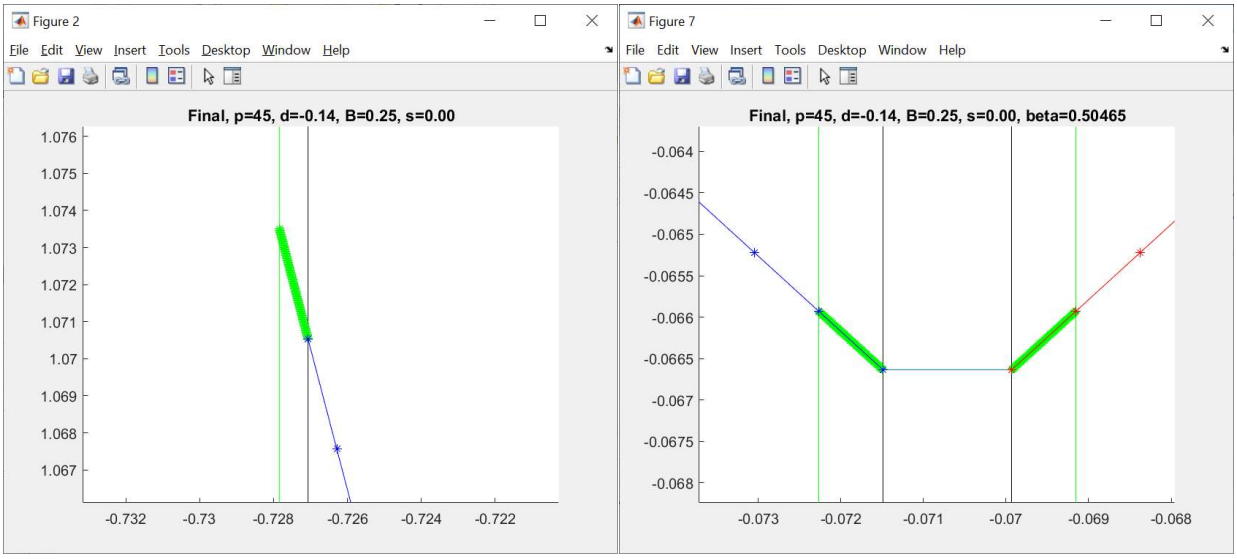

As we can see in the right plot, the space between data points (red and blue asterisks) is nearly as large as the width of the concentrator's base. To increase the accuracy of InterX, we therefore fill in the space between the crucial regions near the top and base of the concentrators, with several more points (green asterisks, which appear as a thick green line).

Points per sidewall	Max Height Factor
1,000	0.504652481033443
10,000	0.505974452617506
1,000 (extension method)	0.504652481033443
10,000 (extension method)	0.505902850545451
100,000 (extension method)	0.506030983592950
1,000,000 (extension method)	0.506031240163057

The above table shows the calculated maximum height factors for both methods, at different resolutions. The first two entries were calculated using a conventional un-filled concentrator. The other four entries were calculated with normal sidewall resolution of 1000 points, but with 1000 to 1000000 points filled into the crucial regions. The accuracy increased as the resolution increased, which was the expected result.

It should also be noted that this level of accuracy is not possible without filling in points using this method. InterX creates a matrix from the input data points. If the entire concentrator had a constant extremely high resolution, this matrix would be too large for Matlab to compute, given memory constraints. It would also take orders of magnitude longer than this method, due to the increased number of potential intersections which have to be checked.